

High-precision numerical simulation for effect of casting speed on solidification of 40Cr during continuous billet casting

Y. Chen, Z. Peng, L. Wu, L. Zhao, M. Wang, Y. Bao

In order to study the effects of casting speed on the solidification process and optimize the process to reduce defects, a high-precision simulation model of solidification and heat transfer of square billet based on nailing test and temperature measurement is presented. The experiments have proven that values calculated by the model fit well the measured values and the relative error is maintained less than 2%. Some new rules about the relationships among casting speed, solidification end point and shell thickness are proposed in the paper for the first time.

Keywords: 40Cr - Continuous casting - Solidification - Simulation model

Model Description and Formulation

Heat Transfer Equation

To simplify the calculations, following assumptions are made based on the actual situation [2]: (1) Billet heat transfer process is simplified two-dimensional unsteady heat transfer. This is quite commonly adopted considering the length of the billet is very large compared to its cross section size. (2) Latent heat released during solidification is dealt with by the way of equivalent heat, since carbon steels usually have large crystallization temperature range. (3) Effect of convective motion in the liquid hole on heat transfer is dealt equivalently by increasing thermal conductivity. (4) Steel thermal physical parameters are only related to temperature, is not related to spatial location. (5) Effect of mold oscillation on the solidification process

is ignored, for it has no significant thermal effect. Based on the assumptions, differential equation of billet solidification is derived:

$$\rho c_p \frac{\partial T}{\partial t} = \frac{\partial}{\partial x} \left(\lambda \frac{\partial T}{\partial x} \right) + \frac{\partial}{\partial y} \left(\lambda \frac{\partial T}{\partial y} \right) \quad (1)$$

where ρ is the density, $\text{kg} \cdot \text{m}^{-3}$; c_p is the specific heat, $\text{J} \cdot (\text{kg} \cdot ^\circ\text{C})^{-1}$; T is the temperature, $^\circ\text{C}$; t is the time, s ; λ is thermal conductivity, $\text{W} \cdot (\text{m} \cdot ^\circ\text{C})^{-1}$.

Initial condition:

$$T(x, y, 0) = T_c \quad (2)$$

Boundary Conditions [3,4]:

(1) Billet center:

$$\lambda \frac{\partial T}{\partial x} \Big|_{x=D/2, t \geq 0} = 0; \quad \lambda \frac{\partial T}{\partial y} \Big|_{y=D/2, t \geq 0} = 0 \quad (3)$$

(2) Billet surface:

$$\lambda \frac{\partial T}{\partial x} \Big|_{x=0, t \geq 0} = q_s; \quad \lambda \frac{\partial T}{\partial y} \Big|_{y=0, t \geq 0} = q_s \quad (4)$$

$$\text{Crystallize: } q_s = A - B\sqrt{t} \quad (5)$$

$$\text{Air zone: } q_s = \varepsilon\sigma[(T_s + 273.15)^4 - (T_a + 273.15)^4] \quad (6)$$

Secondary cooling zone:

$$q_s = h(T_s - T_w) + \varepsilon\sigma[(T_s + 273.15)^4 - (T_a + 273.15)^4] \quad (7)$$

Chen Ya-nan, Peng Zun, Zhao Li-hua, Bao Yan-ping
State Key Laboratory of Advanced Metallurgy-University of Science and Technology Beijing, Beijing 100083, China

WANG Min

National Engineering Research Center of Flat Rolling Equipment, University of Science and Technology Beijing, Beijing 100083, China

WU Lin

Central Iron & Steel Research Institute, Beijing 100081, China

Corresponding author e-mail: baoy@ustb.edu.cn

where q_s is surface heat flux, $W \cdot m^{-2}$; A, B is constant; ε is radiation coefficient, 0,8; σ is Boltzmann constant, $5.67 \times 10^{-8} W \cdot (m^2 \cdot K^4)^{-1}$; T_s, T_w, T_a are the slab surface temperature, cooling water temperature and ambient temperature respectively, $^{\circ}C$; h is heat transfer coefficient in secondary cooling zone $W \cdot (m^2 \cdot ^{\circ}C)^{-1}$.

The heat transfer coefficient in secondary cooling zone is one of the most important parameters to describe the heat transfer effect in secondary cooling zone. The relationship of heat transfer coefficient and the water flow density is shown in Table 1. The form of these equations is basically the same as in the references[5~8]. However, parameters were modified to match the results of both the nail-shooting experiments and the measured surface temperature listed in part 2. Considering that the properties of steel and the calculation method were fixed, the boundary condition was the most influential factor. Therefore, modification of these equations should be acceptable according to measured shell thickness and surface temperature.

Section	150 mm x 150 mm
Foot roller segment	$hW = 0.32 \times 0.341$
First segment in secondary cooling zone	$hW = 0.3 \times 0.321$
Second segment in secondary cooling zone	$hW = 0.28 \times 0.312$
Third segment in secondary cooling zone	$hW = 0.26 \times 0.292$

Tab. 1 - The relationship of Heat transfer coefficient and the flow-density

The real cooling behavior in secondary cooling zone is that the billet surface temperature decrease under the spray zone, while billet surface temperature increase outside the region, considering the number of nozzles and spray cooling range [9]. As a result, the slab surface outside the spray zone is dealt by radiation heat transfer as the formula (6), while water flow density of slab surface in the spray zone is calculated by formula (8), combining nozzle parameters shown in Table 2.

$$W = 1000Q_w / (N_i \cdot \pi \cdot (\frac{d_w}{2})^2) / 3600 \quad (8)$$

$$d_w = 2d_{bs} \left(\tan \frac{\Omega}{2} \right) \quad (9)$$

Where W is water flow density, $L \cdot (m^2 \cdot s)^{-1}$; Q_w is water volume, $m^3 \cdot h^{-1}$; N_i is numbers of nozzles; d_w is the diameter of spray, m; d_{bs} is distance between the nozzle and the surface of the slab, m; Ω is nozzle angle.

Model Parameters

Chemical composition of 40Cr steel is shown in Table 3. The temperature of solid-liquid phase line is calculated by empirical formula. The liquidus temperature is 1495 $^{\circ}C$ and the solidus temperature is 1433 $^{\circ}C$. The solid phase

Segment	Rows of nozzles	Numbers per row	Flat / Arc surface	nozzle angle	Distance from surface/mm	Diameter of spray/mm
Foot roller	2	2	Arc	60	115	132.8
	2	2	Flat	60	115	132.8
First	6	1	Arc	60	104	120.1
	6	1	Flat	60	104	120.1
Second	7	1	Arc	60	106	122.4
	7	1	Flat	60	106	122.4
Third	6	1	Arc	60	106	122.4
	6	1	Flat	60	106	122.4

Tab. 2 - Nozzles parameters

density is taken as $7434 kg \cdot m^{-3}$; the liquid phase density is taken as $6847 kg \cdot m^{-3}$; the two-phase region density is taken as $7134 kg \cdot m^{-3}$. Latent heat of solidification is dealt by the equivalent heat capacity, and 40Cr latent heat is taken as $272 kJ \cdot kg^{-1}$, compared with specific heat of solid phase $647 J \cdot (kg \cdot ^{\circ}C)^{-1}$ and specific heat of liquid phase $828 J \cdot (kg \cdot ^{\circ}C)^{-1}$. The thermal conductivity of solid phase is $30 W \cdot (m \cdot ^{\circ}C)^{-1}$, while the thermal conductivity of liquid phase is larger 1 to 4 times than solid phase, and two-phase region is the average value between solid phase and liquid phase. Basic parameters of caster: casting machine radius 8m, casting machine metallurgical length 26m, crystallizer effective length 0.8m, foot roller length 0.363m, length of first segment in secondary cooling zone 0.989m, length of second segment in secondary cooling zone 1.695m, length of third segment in secondary cooling zone 2.465m.

Element	C	Si	Mn	P	S	Cu	Ni	Cr
Content	0.405	0.27	0.65	0.0225	0.0225	0.18	0.27	0.95

Tab. 3 - Chemical composition (in mass pct) of 40Cr

Model Solution and Verification

Combined with model and parameters above, temperature field and solidified shell thickness can be obtained by the calculation program, which is developed by VB.net. The model is verified by nailing test and temperature measurement [10]. Nail shooting is one of the best ways to measure the thickness of the steel solidified shell, is easy to operate, and is reliable [11]. Sulphur carried in the steel nail is used as a tracer agent in nail shooting to measure the solidified shell thickness of the billet. During casting the steel nail was shot into the billet perpendicular to the surface by a nail shooting gun (as shown in Fig. 1). The nails had sufficient momentum to penetrate the solid shell and the tips would melt in the liquid steel. In this way, the sulphur element was quickly distributed into the molten steel. According to the morphology of the steel nail, the thickness of the solidified shell can be measured. The steel nails used were made of steel 60Si2MnA and the chemical composition is shown in Table 4. The calculated melting point of the steel nails is 1460~1490 $^{\circ}C$.



Fig. 1 - Nail shooting gun

Element	C	Si	Mn	Cr	Other
Content	0.56~0.64	1.60~2.00	0.60~0.90	≤0.35	—

Tab. 4 - Chemical composition (in mass pct) of steel nails

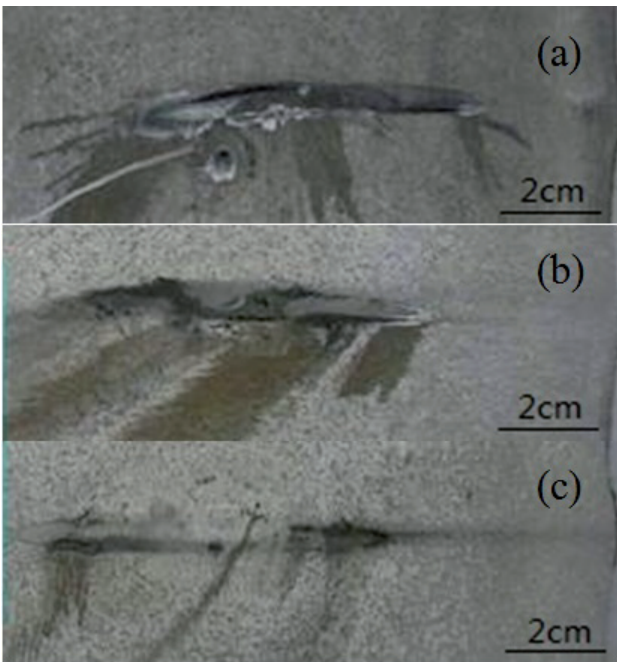


Fig. 2 - Photo of etched pin-shooting samples with different casting speed.
(a) 2.10m/min; (b) 2.40m/min; (c) 2.47m/min

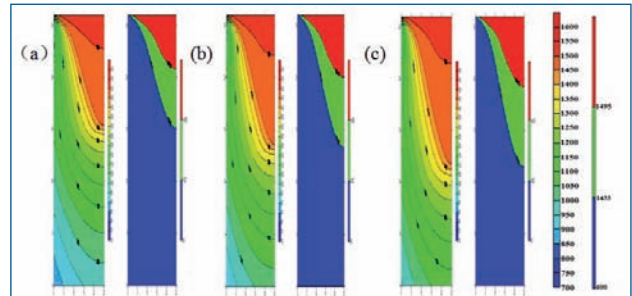


Fig. 3 - Temperature field and solid-liquid phase partition of longitudinal section with different casting speed. (a) 1.9m/min; (b) 2.1m/min; (c) 2.3m/min

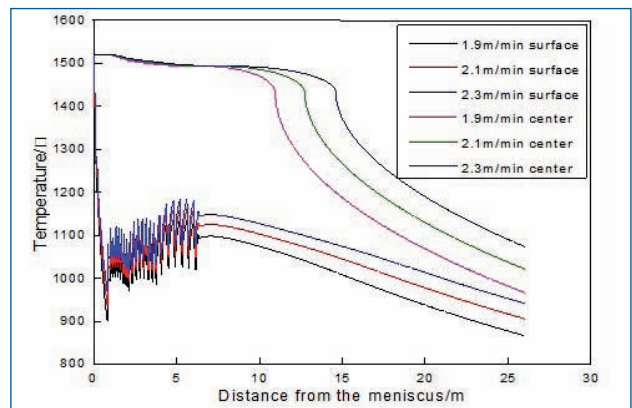


Fig. 4 - Effect of casting speed on temperature of billet

steel grade	Pouring Temperature /°C	Casting speed /m·min ⁻¹	Flow rate of mold / (m ³ /h)	Flow rate of foot zone / (m ³ /h)	Flow rate of 1 st zone / (m ³ /h)	Flow rate of 2 nd zone / (m ³ /h)	Flow rate of 3 rd zone / (m ³ /h)
	1521	2.01	122.2	5.19	5.56	4.81	3.00
	1521	2.10	122.3	5.36	5.85	5.05	3.16
40Cr	1520	2.4	122.3	6.22	6.65	5.76	3.55
	1518	2.47	122.5	6.4	6.84	5.93	3.66

Tab. 5 - Validation tests conditions

In this study, the rivet nail-shooting position was the middle point of right surface 10.34m away from meniscus. Meanwhile, surface temperature at the same point was also measured by infrared thermometer for over 100s and recorded every 0.5s. The validation tests conditions are shown in Table 5. After the nail-shooting sample was lathed, etched in hot hydrochloric acid for 30min and photographed, shell thicknesses were measured by pixels in pictures, as shown in Fig. 2. Model predictions are listed and compared with experiment results in Table 6. The results show that values calculated by the model fit well the mea-

sured values and the relative error is maintained less than 2%. Thus, the model was proved to be highly accurate.

MODEL RESULTS AND DISCUSSION

Effects of casting speed on the temperature field and solidification process

Temperature field and solid-liquid phase partition of longitudinal section are shown in Fig. 3 when the casting speed was taken 1.9, 2.1, 2.3 m/min, separately [12]. Fig. 3 shows visibly that with the casting speed increases, the isotherms moves to the casting direction, liquid phase re-

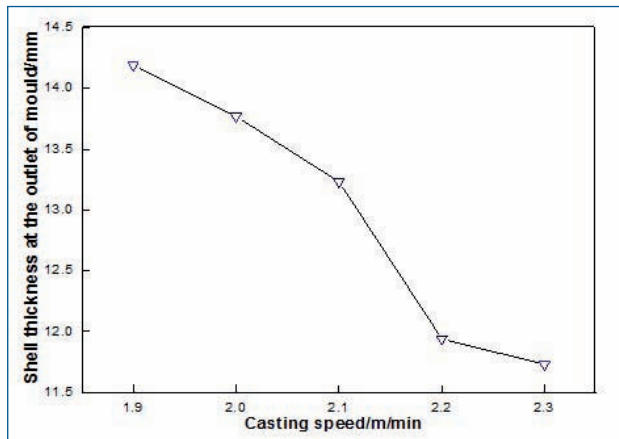


Fig. 6 - Shell thickness at the outlet of mould with different casting speed

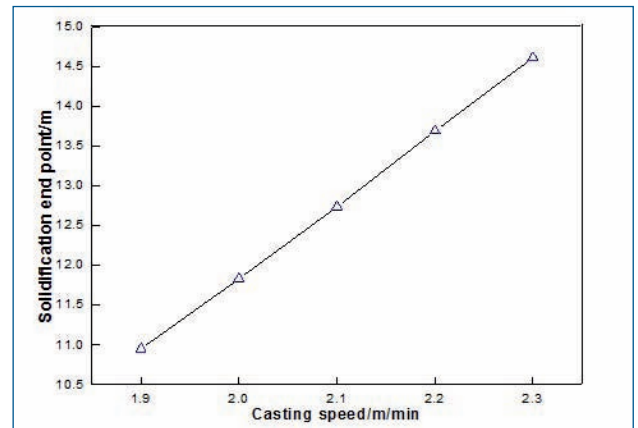


Fig. 7 - Solidification end point with different casting speed

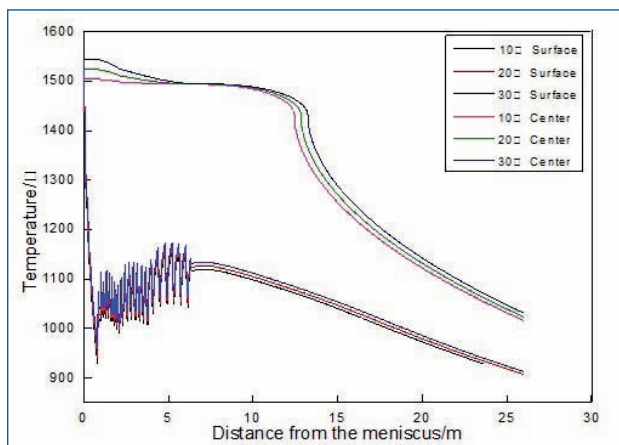


Fig. 8 - Effect of superheat on temperature of billet

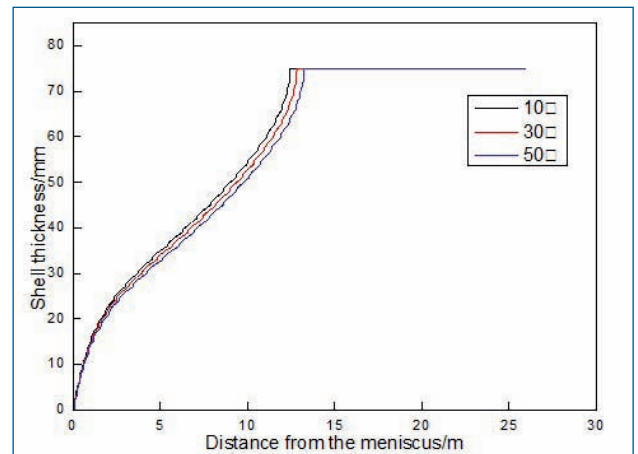


Fig. 9 - Effect of superheat on thickness of shell

Casting speed/ m·min ⁻¹	Measured results/mm	Calculated results/mm	Error,%
2.10	56.4	55.7	1.24
2.4	51.0	50.2	1.57
2.47	44.8	43.9	2.01

Tab. 6 - Comparison between measured and calculated shell thickness

Casting speed/ m·min ⁻¹	Measured results/°C	Calculated results/°C	Error,%
2.01	1090	1100	0.92%
2.10	1100	1115	1.36%

Tab. 7 - Comparison between measured and calculated surface temperature

gion and two-phase region expanded, liquid core length increases significantly. Effects of casting speed on temperature of billet and thickness of shell are shown in Fig. 4 and Fig. 5. As shown in the figures, when casting speed increase by 0.1m/min, middle temperature of the surface at the outlet of third segment in secondary cooling zone increase 13.75°C, the center temperature in the crystallization zone and the secondary cooling zone almost has no change, but significantly increases in the air region, solidification end point lengthens 0.92m or so. It can be seen from Fig. 6 and Fig. 7 that the solidification end point meets approximately linear relationship with casting speed. The shell thickness at the outlet of mould doesn't meet approximately linear relationship with casting speed, and the shell thickness will reduce sharply with the increase of casting speed from 2.1m/min to 2.2 m/min.

Effects of superheat on the temperature field and solidification process

Effects of superheat on temperature of billet and thickness of shell are shown in Fig. 8 and Fig. 9. As shown in the figures, superheat almost has no effect on slab surface temperature, but has a certain impact on center temperature at the early and late period of the solidification

	Original Method		Improved Method	
	Measured value/°C	Predicted value/°C	Measured value/°C	Predicted value/°C
Corner temperature	960	940	979	953
Middle surface temperature	1090	1100	1098	1103

Tab. 8 - Comparison between original method and improved method

process. Superheat has little effect on the growth of shell thickness, but has effect on shell thickness at the outlet of the mold and solidification end point to some extent. When superheat increase 10 °C, shell thickness at the outlet of mold decrease 0.44 mm by average, solidification end point extended about 0.20m.

APPLICATION IN THE PLANT OPERATION

The model has been applied to plant operation at steelmaking plant of Hangzhou Iron and Steel Group to predict the temperature variation and solidification process of slab. In one case, the temperature needs to be improved on a small scale in order to decrease some defects, such as corner cracks and so on. To realize temperature improved on a small scale, the model was used to investigate the effects of operation parameters on slab temperature. The simulated results show that corner temperature can be improved by 13°C (Table. 8) if the flow rates in secondary cooling zone decrease by 10% (Improved Method). The practical production result shows that corner temperature improved about 19°C when the flow rate was by 10% at cast speed of 2.01m/min Experimental results were similar with the predicted results, so the model can be applied to plant operation. When the improved trial method finally turned to regular process in winter, the flow rate in the third segment was further reduce by 20%. Combined this optimized cooling strategy and more strict Nitrogen control measures in RF process, severe batch corner cracking problems seldom happened again in winter.

CONCLUSIONS

- (1) The experiments of temperature and shell thickness measurements have proven that values calculated by the model fit well the measured values and the relative error is maintained less than 2%.
- (2) Casting speed is the most important factor in determining the temperature field and solidification process of 40Cr during Continuous Billet Casting. With the increase of casting speed by 0.1 m/min, the solidification end point extended about 0.92 m. The solidification end point meets approximately linear relationship with casting speed. The shell thickness at the outlet of mold doesn't meet approximately linear relationship with ca-

sting speed, and the shell thickness will reduce sharply with the increase of casting speed from 2.1m/min to 2.2 m/min.

- (3) Superheat has some effects on the solidification process to some extent. When superheat increase 10 , shell thickness at the outlet of mold decrease 0.44 mm by average, solidification end point extended about 0.20m.

ACKNOWLEDGMENT

This research was supported financially by the National Natural Science Foundation of China (No.51274029), Doctoral Fund of Ministry of Education of China (No.20130006110023) and State Key Laboratory of Advanced Metallurgy Foundation (No.41602014).

REFERENCES

- [1] Richard A, Kai L, Atul K, et al. A Transient Simulation and Dynamic Spray Cooling Control Model for Continuous Steel Casting. *J Metall Mater Trans. B*, 2003, 34B:297
- [2] Ya M, Brian G T, Heat-Transfer and solidification model of continuous slab casting: CON1D. *J Metall Mater Trans B*, 2003, 34B:685
- [3] Park H S, Nam H, Yoon J K. Numerical analysis of fluid flow and heat transfer in the parallel type mold of a thin slab caster. *J ISIJ Int*,2001, 41(9): 974
- [4] Yang H L, Zhao L G, Zhang X Z, et al. Mathematical simulation on coupled flow, heat, and solute transport in slab continuous casting process. *J Metall Mater Trans B*,1998,29B:1345
- [5] Laitinen E, Neittaanmaki P. On numerical simulation of the continuous casting process. *J J Eng Math*.1988,22:335
- [6] Yang H L, Zhao L G, Zhang X Z, et al. Mathematical simulation on coupled flow, heat, and solute transport in slab. *J Metall Mater Trans. B*,1998,29B:1345
- [7] Yoon J K.A fully-coupled analysis of fluid flow, heat transfer, solidification and deformation behavior in continuously cast beam blank. China-Korea Joint: Symposium on Advanced Steel Technology for Future Industry, Beijing, China, 1999:34.
- [8] Kondo O, Hamada K. New dynamic spray control system for secondary cooling zone of continuous casting machine. 1993 Steelmaking Conference Proceedings,1993, 309.
- [9] López A R, López R A, Pardavé M P. Simulation of heat transfer in steel billets during continuous casting. *J INT J MIN MET MATER*.2010,17(4):403
- [10] Liu J J, Liu J H, Wu H J, et al. Numerical simulation of solidification process for continuous casting large size steel square billet containing 0.45%C. *J Foundry.Technol*,2011,32(2):259
- [11] Long M J, Chen D F, Wang Q X, et al. Determination of CC slab solidification using nail shooting technique. *Ironmak & Steelmak*, 2012,39(5):370
- [12] López A R, López R A, Bello A K, et al. Simulation factors of steel continuous casting. *J INT J MIN MET MATER*.2010,17(3):267